The impact of the nano-pore filling on the performance of organosilicon-based moisture barriers

Thin Solid Films 595 (2015) 251–257

Contents lists available at ScienceDirect

Thin Solid Films

journal homepage: www.elsevier.com/locate/tsf

The impact of the nano-pore filling on the performance of organosilicon-based moisture barriers

Alberto Perrotta [a,b,*], Gianfranco Aresta [a], Erik R.J. van Beekum [a], Jurgen Palmans [a], Peter van de Weijer [d], M.C.M. Richard van de Sanden [c], W.M.M. Erwin Kessels [a,e], Mariadriana Creatore [a,e]

[a] Department of Applied Physics, Eindhoven University of Technology, P.O. Box 513, 5600 MB Eindhoven, The Netherlands
[b] Dutch Polymer Institute (DPI), P.O. Box 902, 5600 AX Eindhoven, The Netherlands
[c] Dutch Institute for Fundamental Energy Research (DIFFER), P.O. Box 1207, 3430 BE Nieuwegein, The Netherlands
[d] Philips Research, High Tech Campus 4, 5656 AE Eindhoven, The Netherlands
[e] Solar Research SOLLIANCE, High Tech Campus 5, 5656 AE Eindhoven, The Netherlands

ARTICLE INFO

Available online 23 May 2015

Keywords:
Initiated chemical vapor deposition
Moisture barriers
Ellipsometric porosimetry
Nano-pore filling
Silicon dioxide

ABSTRACT

Promising results in terms of moisture and oxygen permeation barrier properties have been reported for organic/inorganic multilayers, but the impact of the organic interlayer on the overall barrier performance is still under discussion. It is generally accepted that the organic interlayer acts as a smoothening layer, allowing for the decoupling between defects/pinholes present in the polymer substrate and the inorganic layer. It is, however, also hypothesized that the organic interlayer infiltrates into the nano-pores present in the inorganic barrier layer, therefore affecting the barrier properties at microstructural level. In the present work, the moisture permeation barrier performance of SiO_2/organosilicon multilayers deposited by means of initiated- and plasma enhanced-chemical vapor deposition is investigated. Calcium test measurements were used to discriminate between the overall water permeation (*effective* water vapor transmission rate, WVTR) through the layer and the permeation through the matrix porosity (*intrinsic* WVTR). The improvement in terms of *intrinsic* barrier performance was found to correlate with the residual nano-porosity content, due to the filling/infiltration of the organosilicon monomer in the SiO_2 nano-pores. However, such improvement upon the deposition of the organosilicon interlayer is limited to a factor four. These results, in combination with the analysis of the local defects present in the multilayer structure, lead to the conclusion that the main contribution of the organosilicon interlayer to the overall barrier performance is the decoupling of the above-mentioned local defects/pinholes.

1. Introduction

The state-of-the art in the field of ultra-high moisture diffusion barriers is represented by a multi-layer solution in which an inorganic (*e.g.*, Al_2O_3, Si_3N_4 or SiO_2) thin film (<100 nm) barrier is coupled with an organic (generally an acrylate- or organosilicon-based polymer) interlayer, with thickness ranging from hundreds of nanometers to micrometers[1] It is worth addressing that, next to the multilayer solution, inorganic nano-laminates are growing in importance in the moisture barrier field. This solution consists of alternated ultra-thin inorganic layers (*e.g.*, ZrO_2, TiO_2, Al_2O_3) [55]. [1]. This approach has led to water vapor transmission rate (WVTR) values in the 10^{-6} g m^{-2} day^{-1} regime [2–4], therefore suitable for the encapsulation of high-end devices, such as thin film solar cells and flexible organic light emitting diodes [5].

In multilayer barrier systems, the inorganic/organic dyads are generally deposited by a hybrid approach: sputtering or plasma enhanced-chemical vapor deposition (PE-CVD) of the inorganic barrier layer, in combination with flash evaporation/condensation of the organic monomer, and followed by curing/polymerization [2,6–9]. Additionally, different deposition approaches such as atomic layer deposition (ALD) in combination with molecular layer deposition [10–14], and all PE-CVD developed multilayers have been reported in literature [15–18]. Coclite et al. [19] reported on the deposition of multilayers based on organosilicon chemistry, in which the inorganic barrier layer is deposited by means of PE-CVD and the organic interlayer is deposited by means of initiated-CVD (i-CVD) [20–22]. Recently, Spee et al. reported on the deposition of SiN_x/poly-glycidylmethacrylate/SiN_x, where the inorganic layer was deposited by hot wire chemical vapor deposition (HWCVD) and the organic layer by i-CVD [4]. The appeal of the i-CVD technique is its compatibility with vacuum systems and the full retention of the monomer chemistry, similarly to liquid phase polymerization processes

* Corresponding author at: Department of Applied Physics, Eindhoven University of Technology, P.O. Box 513, 5600 MB Eindhoven, The Netherlands. Tel.: +31 402474095; fax: +31 402456442.
E-mail addresses: a.perrotta@tue.nl, m.creatore@tue.nl (A. Perrotta).

[1] It is worth addressing that, next to the multilayer solution, inorganic nano-laminates are growing in importance in the moisture barrier field. This solution consists of alternated ultra-thin inorganic layers (*e.g.*, ZrO_2, TiO_2, Al_2O_3) [55].

http://dx.doi.org/10.1016/j.tsf.2015.05.026
0040-6090/

[23,24]. Furthermore, compared to the classical flash evaporation/polymerization method, i-CVD is well acknowledged for its high conformality. This is guaranteed by the polymerization mechanism, which occurs only at the substrate surface.

The need for a multilayer barrier technology derives from the limits associated with single inorganic layers, their permeation barrier level being ultimately controlled by the presence of defects. These defects range in diameter from the nanometer-scale (*i.e.*, well above the water kinetic diameter of 0.27 nm), up to substrate/process-induced macro-defects (*e.g.*, pinholes and particles with a diameter in the range of micrometers) [25]. The successful application of a multilayer is generally attributed to the smoothening effect associated with the organic polymer layer, which allows for a more controlled growth of the subsequent inorganic barrier [2,26,27]. Additionally, Graff et al. [28] carried out numerical simulation studies and reported on the development of a "tortuous" path for the permeant molecule upon the application of a multilayer. Hence, the organic interlayer was found to lower the overall barrier permeability by decoupling the pinholes/defects present on the inorganic layers.[2]

Although defects/pinholes represent an unhindered path for the permeant molecule [29,30], the kinetic diameter of the water molecule allows it to permeate through (sub-)nm sized pores, *i.e.*, the nano-porosity or free volume of the inorganic matrix. Affinito and Hilliard [26] highlighted that the estimated area density of the nano-pores can be approximately up to 15–20 times larger than the one of the defects/pinholes, leading to a higher permeation flux than through macro-defects. Therefore, an additional role of the organic interlayer was proposed, *i.e.*, the infiltration of the organic monomer in its liquid phase into the nano-porosity of the inorganic barrier layer underneath. Eventually, this infiltration is expected to influence the local water permeation through the filled pores. Recently [31], we reported on the experimental evidence for the infiltration of an i-CVD monomer into the nano-pores (from 1 to 2 nm in pore size) of single PE-CVD SiO_2 barrier layers during the initial stages of the polymerization process. These studies confirmed that the hypothesis of Affinito et al. [26] also applies for a CVD-based process.

The present work focuses on PE-CVD/i-CVD multilayers and addresses the contribution of the afore-mentioned infiltration in the nano-porosity to the *intrinsic* moisture permeation barrier performance. In order to discern between the effect of the filling/infiltration (affecting the porosity of the matrix of the barrier layer) and the decoupling effect (associated with the defects/pinholes in the layer), both *effective* and *intrinsic* WVTR were determined by means of the calcium (Ca) test [32]. The *effective* WVTR refers to the overall oxidation of the Ca-layer, whereas the *intrinsic* WVTR excludes the defects/pinholes as far as they are visible in the Ca test as white spots. More details on the test can be found in the experimental section.

The relative content of porosity accessible to the organic monomer was monitored by ellipsometric porosimetry (EP) [33–37]. EP is based on the adsorption of a probing molecule on the layer, which leads to a change in the layer optical properties, and these are followed by means of spectroscopic ellipsometry (SE). The variation of the optical properties as function of the ratio between the partial pressure (P_M) and the vapor pressure (P_{sat}) of the monomer at constant temperature results in the classical adsorption/desorption isotherm [35,38,39], which provides information on the microstructure of the layer and an estimation of the (average) pore size.

The paper is organized as follows: in the experimental section a description of the deposition chamber is provided, together with the diagnostic techniques, *i.e.*, IR spectroscopy, *in situ* spectroscopic ellipsometry, EP measurements, and Ca test. The section Results and Discussion addresses the comparison in terms of chemistry and barrier properties of the i-CVD/PE-CVD and all PE-CVD developed multi-layers. Differences in the barrier properties of the two systems are investigated and correlated to the extent of monomer infiltration, measured by means of *in situ* ellipsometry studies. Then, a series of PE-CVD SiO_2 films showing a wide range of porosity is studied in terms of their nano-porosity content and *intrinsic* barrier properties. First, the nano-porosity accessible to the organosilicon monomers is characterized by *in situ* spectroscopic ellipsometry for the two extremes of the series. Next, the effect of the infiltration of the organosilicon monomer in the porosity of the (barrier) layer is investigated for the whole series and justified on the base of the nano-pore content.

2. Experimental details

All the layers were deposited without breaking the vacuum in a custom-built setup which allows for thin film deposition by means of both PE-CVD and i-CVD approaches [31,37]. The wire system for i-CVD is mounted on a magnetic movable arm, and during the i-CVD process it is inserted into the deposition chamber at a distance of 2 cm from the substrate holder. 1,3,5-trivinyl-1,3,5-trimethylcyclotrisiloxane (V_3D_3, purity > 95%, Gelest, $d_{V_3D_3} = 1$ nm) was adopted for the i-CVD process after 3 freeze–thaw cycles. The initiator (di-tert-butyl peroxide: TBPO, purity > 98%, Aldrich) is mixed together with the monomer in a buffer and injected into the deposition chamber through a ring placed above the grid. The grid is connected to a custom-built DC power supply system, equipped with a feed–loop system. During the PE-CVD process, the grid is transferred from the deposition chamber to a load-lock chamber. The SiO_2 and $SiO_xC_yH_z$ layers are deposited by means of a parallel plate RF-plasma, and V_3D_3 is adopted as precursor. Before each deposition, the chamber is evacuated to a pressure of 10^{-5} mbar, and the setup is arranged for either the i-CVD or PE-CVD process. Table 1 reports the experimental conditions for all the processes. In the case of the poly(V_3D_3) layer, the conditions were chosen according to previous studies aimed at the deposition of stable, smooth layers with a high conversion (*i.e.*, >85%) of vinyl groups [40]. The setup is equipped with spectroscopic ellipsometry (SE)-compatible windows to study the film growth during each process.

In order to further investigate the infiltration of the organic polymer into the matrix of the inorganic layer, another organosilicon monomer was chosen with a dimension smaller than V_3D_3, 1,1,3,5,5-pentamethyl-1,3,5-trivinyltrisiloxane (TVTSO, purity > 95%, Gelest, $d_{TVTSO} = 0.85$ nm). First, the i-CVD process was optimized in order to find a process window for stable, dense polymers. The polymerization and polymer characteristics were investigated by following the same procedure adopted for V_3D_3 and explained in Ref. [40]. For the TVTSO monomer, a process window was identified at P_M/P_{sat} values below 0.2.

2.1. Film growth study and single layer characterization

The film growth process was followed by means of *in situ* SE, at an angle of incidence of 71.5°, wavelength range of 245–1000 nm, 1.6 nm resolution, by using a J.A. Woollam Co. M-2000F ellipsometer. The data analysis was performed by using the J.A. Woollam Complete EASE™ software, and the mean squared error between the experimental data and the model is minimized by adjusting the fit parameters using the Levenberg-Marquardt algorithm. The optical model for the film growth study consists of a Si substrate, native SiO_2 (~1.5–2 nm), Cauchy and Cauchy coupled with the Urbach absorption tail functions for the SiO_2 and the organosilicon interlayer ($SiO_xC_yH_z$, poly(V_3D_3) and poly(TVTSO)), respectively, according to Eqs. (1)–(2):

$$n(\lambda) = A + B/\lambda^2; k(\lambda) = 0 \tag{1}$$

$$n(\lambda) = A + B/\lambda^2 + C/\lambda^4; k(\lambda) = \alpha \cdot e^{\beta[12400(1/\lambda - 1/\gamma)]} \tag{2}$$

[2] It is worth mentioning that in this simulation it is assumed that the moisture permeation occurs only through the defects/pinholes present in the barrier layer which is considered elsewhere as impermeable.

Table 1
Experimental conditions for the multilayer deposition process.

	i-CVD/poly(V_3D_3)	i-CVD/poly(TVTSO)	PE-CVD/$SiO_xC_yH_z$	PE-CVD/SiO_2
V_3D_3 flow (sccm)	10	3	0.7	0.7
d-TBPO flow (sccm)	2	1	–	–
Ar flow (sccm)	–	-	100	70
O_2 flow (sccm)	–	-	–	35
Pressure (mbar)	0.7	0.1	0.45	0.3
Plasma power (W)	–	-	50	140–250
T_{grid} (°C)	400	290	–	–
T_{sub} (°C)	60	40	100	100

in which *A*, *B* and *C* are the Cauchy fitting parameters, and α and β the Urbach function parameters used to fit the absorption tail, due to the carbon present in both i-CVD and $SiO_xC_yH_z$ layers.

The chemistry of the deposited layers is investigated by means of Fourier Transform Infrared (FT-IR) measurements carried out with a Bruker Tensor 27 spectrophotometer. The FT-IR spectra are acquired in the range of 400 cm^{-1}–4000 cm^{-1}, with a resolution of 4 cm^{-1}, and 256 scans per average. Before the spectra acquisition, the spectrometer is purged for 15 min with N_2 to minimize the effect of H_2O and CO_2 absorption. All the spectra were baseline corrected and normalized by the thickness of the layer.

2.2. Ellipsometric porosimetry

The open porosity of the SiO_2 layer was studied by means of EP measurements with V_3D_3 ($d_{V_3D_3} = 1$ nm) and TVTSO ($d_{TVTSO} = 0.85$ nm) as probe molecules, and He as buffer gas, under the conditions described in Table 2.

After loading the SiO_2 sample, the chamber was evacuated overnight in order to remove the adsorbed water due to the layer exposure to ambient. The refractive index value of the SiO_2 layer after evacuation is taken as starting point for the adsorption measurements (*i.e.*, n_0). Then, the probe molecule and He are injected into the chamber at the base pressure of 10^{-5} mbar, and the pressure is then increased by equilibrium steps in order to scan the entire P_M/P_{sat} range from 0 to ~1. The monomer adsorption on the SiO_2 layer is monitored in real time by means of *in situ* SE measurements. As shown later, all the studied layers are characterized by the detection of residual nano-porosity, followed by multilayer adsorption. Therefore, in order to represent both effects, the adsorption isotherms are reported in terms of optical thickness as in Eq. (3):

$$n \cdot d = n_{SiO_2} \cdot d_{SiO_2} + n_{probe} \cdot d_{probe} \tag{3}$$

where n_{SiO_2} is the SiO_2 refractive index, d_{SiO_2} is the constant SiO_2 layer thickness, n_{probe} is the probe molecule refractive index, and d_{probe} is its multilayer thickness. The probe multilayer uptake was fitted by adding a Cauchy layer on top of the SiO_2 layer with fixed refractive index of the monomer, and with its thickness being the only fitting parameter.

The variation of the optical properties as function P_M/P_{sat} of the monomer results in an adsorption isotherms. The adsorption isotherms are categorized according to the IUPAC classification [37–39]. A type I isotherm is associated with nano-porous materials (elsewhere also addressed as micro-porous [35,38]) with a narrow distribution of pore sizes and a pore diameter < 2 nm, and a type II isotherm is associated with a non-porous material with multilayer adsorption. As explained later, the investigated layers showed a hybrid type I + II isotherm.

Table 2
Conditions adopted during the EP measurements on the SiO_2 layers.

V_3D_3 or TVTSO flow (sccm)	5
He flow (sccm)	2
T_{sub} (°C)	25
Pressure (mbar)	10^{-5}–0.78
T_{walls} (°C)	80

2.3. Water vapor transmission rate measurements

Water vapor transmission rate (WVTR) measurements are carried out by means of the Ca test according to the procedure described by Nisato et al. [3,32], at a constant temperature of 20 °C and a relative humidity (R.H.) of 50%. For this test, the measured barrier layer is stacked with a 40 nm thick Ca layer. Any changes to the optical transmittance of this Ca layer following exposure to the water vapor can be attributed to oxidation of the Ca to CaO (since CaO is transparent), and therefore, in turn, to permeation of water vapor through the barrier layer. In order to distinguish between the *intrinsic* and *effective* barrier performances, the contribution to the permeation through the nano-pores and defects/pinholes is measured separately. The *intrinsic* WVTR is measured by excluding local white spots from the measurement; these develop due to localized fast oxidation of Ca, associated with the water permeating through a defect or pinhole. In this way, only the permeation through the nano-pores is considered. The *effective* WVTR is instead measured taking into account *both* contributions.

The measurement setup for the Ca test (developed by the Philips Research laboratories) consists of a Philips CL5000M light source with a diffuser for uniform back lighting and a sample holder with mask. A 12 bit Adimex MX12p camera was used to obtain a gray scale image of the sample. The extent of oxidation is determined from the gray scale. A non-transparent black reference from the mask and a white reference from the transparent part of the glass plate were included in every measurement to define the gray scale range and to correct for transparency changes, due to permeation through the barrier film. Two configurations are adopted for the Ca test according to the different substrates on which the barrier systems are deposited. Ca can be deposited first, on glass substrates, followed by the deposition of the barrier system, or it can be deposited directly on the barrier system, if the latter was deposited on a polymer substrate. In the first case, a temporary PE-CVD SiO_x (*intrinsic* WVTR of 10^{-2} g m^{-2} day^{-1}) barrier layer is deposited on the glass/Ca system to avoid oxidation during transportation. The use of the temporary SiO_x layer has no effect on the determined *intrinsic* WVTR values since its barrier performance is one-to-three orders of magnitude lower than the barrier layers under investigation. The comparison in terms of the *intrinsic* WVTR values among the single SiO_2 barrier layers was carried out on the glass/Ca/40-nm-SiO_x/barrier layer configuration. In the second configuration, the barrier is deposited on a glass/polymer(polyethylene naphthalate, PEN) substrate, made by laminating 125-μm-thick PEN (DuPont) foils on 100 cm^2 glass plates. Measurement of the *effective* barrier properties of the multilayers on a PEN substrate was performed using the following configuration: glass/PEN/barrier/Ca/a-SiN_x:H. In this case, the a-SiN_x:H [5] barrier layer is deposited by PE-CVD, and is used to seal the system, since it shows excellent (10^{-6} g m^{-2} day^{-1}) *intrinsic* barrier properties. Note that the PEN/barrier/Ca/a-SiN_x:H systems were delaminated from the glass prior to Ca testing. Determination of the *effective* WVTR values was

performed by taking a weighted average of the transmission through the barrier system matrix and defects/pinholes.

For both configurations, Ca was deposited by thermal evaporation on the glass plates or barrier systems in a structure consisting of either 4 or 9 samples, each divided in 9 squares of 0.25 cm^2, to avoid that the water vapor permeating through one defect would affect the whole area of the samples.[3]

3. Results and discussion

3.1. Single layer comparison

FT-IR measurements were carried out in order to verify the polymerization process by means of i-CVD and PE-CVD techniques and characterize the deposited layers. Fig. 1 shows the comparison between the FT-IR absorption spectra of the i-CVD and PE-CVD layers, normalized by their thickness, together with the liquid V_3D_3 and TVTSO monomer spectra [39]. The monomer functional groups (namely the Si—CH_3 bending absorption band at 1260 cm^{-1} [41,42], and the Si—O—Si asymmetric stretching band, either cyclic at 995 cm^{-1}, or linear 1066 cm^{-1} [43]) are entirely retained in the i-CVD polymer structures, as also shown in Ref. [40], since the vinyl groups are the only units involved in and affected by the polymerization process [41,44,45]. On the contrary, the opening of the cyclotrisiloxane ring into the $SiO_xC_yH_z$ layer spectrum is witnessed by the broadening of the Si—O—Si asymmetric stretching band centered at 1020 cm^{-1}. This stretching band is characterized by a higher wavenumber (1080 cm^{-1}) shoulder associated with short, linear siloxane chains [41,46,47], and by the presence of the O_ySi—H_x stretching at 2100 cm^{-1} [42,47]. The broadening and decrease in intensity of the Si-$(CH_3)_x$ related signal at 1260 cm^{-1} reveals a shift towards a O_xSi-$(CH_3)_y$ chemistry [47–49], due to the fragmentation occurring in the plasma phase.

3.2. Effective barrier performance

The barrier performances of the above-mentioned multilayers deposited on PEN substrates were tested, and the *effective* WVTR values are reported in Fig. 2a. For each system a single SiO_2 layer was deposited as a reference. The 100-nm-thick SiO_2 layer shows already very good *effective* barrier properties, with an average barrier improvement factor (BIF) of 80 with respect to the pristine PEN substrate, superior to other values reported in literature for PE-CVD deposited SiO_2 layers [16,19,50]. When two 100-nm-thick SiO_2 layers are coupled with a 200-nm-thick poly(V_3D_3) layer, the barrier property of the multilayer further improves, with an overall BIF with respect to the pristine PEN of 1000. When the SiO_2 layers are coupled with a 200-nm-thick $SiO_xC_yH_z$ organic interlayer, no barrier improvement with respect to the single SiO_2 layer is observed.

On the basis of what discussed earlier, the influence of the i-CVD and PE-CVD organic interlayers on the *intrinsic* and *effective* barrier performance values is here investigated in terms of monomer infiltration in the nano-porosity and decoupling of defects, respectively. The latter effect is inferred by comparing the defect density[4] evolution, derived from the detected white spots during the Ca test, as shown in Fig. 2b. In the presence of the poly(V_3D_3) interlayer, the defect density is reduced by a factor 5 compared to the single SiO_2 layer, while, in the case of the $SiO_xC_yH_z$ interlayer, no decrease in defect density is reported. This suggests a smoothening/decoupling effect of the poly(V_3D_3) interlayer with respect to the SiO_xC_yH layer, due to the higher conformality of the i-CVD layer [51,52], which leads to a better coverage of the local particles/defects [19].

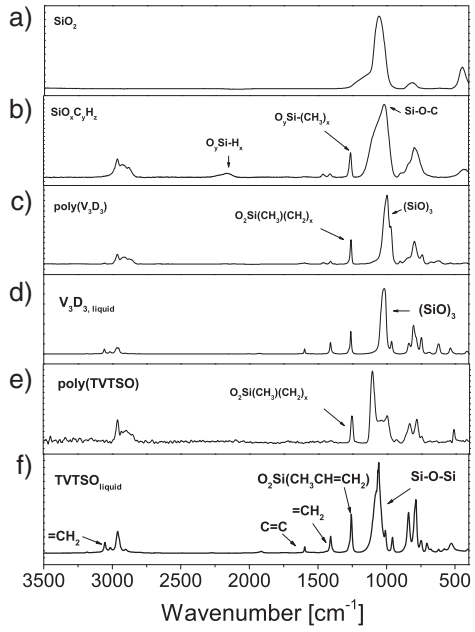

Fig. 1. FT-IR spectra, normalized by the layer thickness, of the a) PE-CVD SiO_2 and b) $SiO_xC_yH_z$ layers, i-CVD, c) poly(V_3D_3) and e) poly(TVTSO). The spectra of the liquid phase organosilicon monomers, d) V_3D_3 and f) TVTSO, are added for comparison.

3.3. Infiltration of the organic interlayer in the SiO_2 layer

The second effect (*i.e.*, the infiltration of the organic interlayer into the nano-porosity of the underlying barrier) is investigated by comparing the poly(V_3D_3) and $SiO_xC_yH_z$ initial growth on the barrier layer, as shown in Fig. 3. For sake of comparison, the optical thickness of the layer is considered. In Fig. 3a, the i-CVD process is monitored: while setting the process pressure value, an uptake of the optical thickness is observed due to V_3D_3 adsorption in the open nano-porosity, as we have already reported in Ref. [31]. The diameter of the V_3D_3 molecule allows it to infiltrate in pores with a size ≥ 1 nm. After the pressure is set to the deposition conditions, the grid is heated and the growth of the i-CVD layer proceeds linearly.

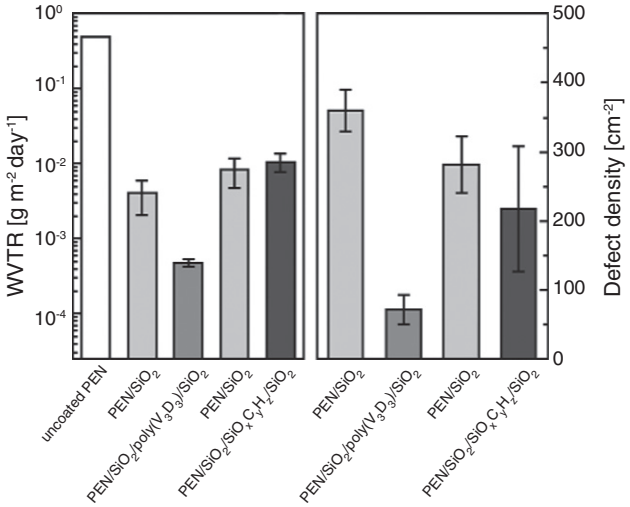

Fig. 2. a) *Effective* WVTR values and b) defect density of the single SiO_2 layer and the i-CVD/PE-CVD and PE-CVD multi-layers.

[3] No effect of a potential side-leakage is taken into account. As a matter of fact, in our measurement configuration, a water molecule diffusing laterally through the barrier to the Ca samples should go through a path in the range of several centimeters, orders of magnitude higher than for a molecule permeating through the barrier system.

[4] The defects present on the surface of the PEN substrate find their origin either in the dust contamination due to lab environment and/or antistatic particles, prior to the deposition process. The defect density can be rather scattered, as shown in Fig. 2b. Therefore, a single SiO_2 barrier layer has been used as a reference for each set of multi-layers.

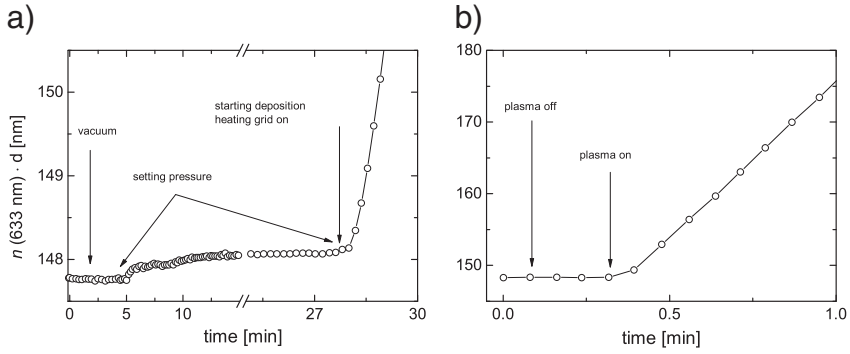

Fig. 3. Initial growth of a) poly(V_3D_3) and b) $SiO_xC_yH_z$ layers on SiO_2 barrier films.

In the case of the PE-CVD process, shown in Fig. 3b, there is no change in the optical thickness prior to the ignition of the plasma, indicating no monomer adsorption in the open porosity of the barrier layer. This difference can be easily interpreted in terms of the P_M/P_{sat} parameter [24], which controls the monomer surface adsorption. In the case of the poly(V_3D_3) layer, P_M/P_{sat} equals 0.113 at 60 °C, while in the case of $SiO_xC_yH_z$ this value is in the order of 10^{-4}. Furthermore, the sticking coefficient of organosilicon radicals generated in the plasma is high, limiting their surface diffusion processes [53,54] and therefore limiting the conformal growth in the open porosity of SiO_2 layer. Hence, it can be expected that only in the case of the i-CVD/PE-CVD multilayer the filling of the nano-pores by the poly(V_3D_3) may play a role in affecting the multilayer barrier properties.

3.4. Nano-porosity characterization in SiO_2 layers

In the previous section, the infiltration of the i-CVD monomer in the SiO_2 layers was demonstrated by replicating the i-CVD experimental conditions. In order to fully characterize the residual nano-porosity of the SiO_2 layers, ellipsometric porosimetry measurements were performed on two SiO_2 layers, which show an *in situ* refractive index value of 1.447 and 1.422 (see Table 3). The layers were deposited under the same experimental conditions in Table 1 and by setting the plasma power at 140 W and 250 W, corresponding to the layer with the lowest and highest refractive index, respectively. These two layers have been chosen because they cover a rather broad range of *intrinsic* barrier performances (see Table 3), as inferred by the correlation earlier presented in [37]. The data reported in Fig. 4 show in both cases that, during the adsorption path, an initial optical thickness uptake develops due to nano-pore filling at very low P_M/P_{sat}, followed by the monomer multilayer adsorption. This behavior corresponds to a hybrid type I–II isotherm.

The nano-pore relative content is determined at the rounded knee, *i.e.*, when the nano-pore filling is complete [37,39], and the values are reported in Table 3. Although the difference in residual open porosity is small, it is reproducible and related to pores accessible to either V_3D_3 and/or TVTSO molecule. The detected porosity points out that TVTSO is able to infiltrate in a larger amount of pores, compared to V_3D_3. Due to the smaller diameter of TVTSO, this infiltration is expected to affect the permeation of water even for barriers not affected by V_3D_3 deposition.

Table 3
Nano-porosity values, as determined by EP measurements, and WVTR values of the different SiO_2 layers deposited by PE-CVD. The *in situ* values of the layer refractive index are also reported.

PE-CVD SiO_2 layer	$n_{in\ situ}$ (633 nm)	Nano-porosity V_3D_3 [%]	Nano-porosity TVTSO [%]	WVTR [g m^{-2} day^{-1}]
Dense	1.447	0.13	0.22	$2\cdot10^{-5}$
Porous	1.422	0.21	0.31	$3\cdot10^{-3}$

3.5. Evaluation of the intrinsic barrier performance

In order to investigate any beneficial effect of the infiltration in the nano-pores by the i-CVD polymers, the *intrinsic* barrier properties of several 100-nm-thick SiO_2 layers, with an *intrinsic* WVTR in the range between $1\cdot10^{-5}$–$3\cdot10^{-3}$ g m^{-2} day^{-1}, were compared with those of SiO_2 layers after deposition of a 20-nm-thick organosilicon layer (Fig. 5). The different SiO_2 layers were deposited under the same experimental conditions reported in Table 1 and by tuning the plasma power in the range between 140 W and 250 W. The organosilicon thickness value of 20 nm has been chosen to guarantee the filling of the open pores present in the SiO_2 layers.

Using V_3D_3 as organosilicon monomer, the infiltration study showed that there is no barrier improvement upon infiltration of the poly(V_3D_3) in the nano-pores for *intrinsic* WVTR values below $3\cdot10^{-4}$ g m^{-2} day^{-1} (Fig. 5). Above this value, an improvement in the *intrinsic* barrier properties is observed upon the deposition of the 20-nm-thick polymer. Under these conditions, however, the BIF is limited to a value of 4. The observed BIF values cannot be attributed to the poly(V_3D_3) *intrinsic* barrier performance by applying the ideal laminate theory [26], since it is in the same order of the PEN substrate barrier level, and therefore negligible with respect to the pristine SiO_2 barrier performance.

The same study was performed with TVTSO. In this case, an improvement was found for barriers showing *intrinsic* WVTR values down to $3\cdot10^{-5}$ g m^{-2} day^{-1}, whereas, below this limit, no improvement in the barrier properties was detected. The difference between TVTSO and V_3D_3 can be explained in terms of molecule diameter, TVTSO being able to infiltrate in smaller pores. Nevertheless, notwithstanding the smaller dimension of the TVTSO molecule, the BIF value was still limited to a factor of 4. This result can be explained by considering that a porosity is present in the SiO_2 layer, not accessible to the organosilicon monomers, but yet accessible to H_2O. In fact, upon exposure to the ambient (R.H. of 40–60%), the refractive index of the layers increases due to the filling of the open pores accessible to water vapor ($d \geq 0.27$ nm). The open porosity was then calculated and found to be 4.3% and 7.4% for the dense and porous SiO_2 layer, respectively, pointing out that the majority of the pores has a diameter smaller than both organosilicon monomers used [37]. Hence, it can be concluded, then, that the presence of these nano-pores and the low mass density of the organosilicon polymers, which not effectively hinder the permeation path of the water molecules, account for the limited BIF improvement upon filling of the barrier nano-pores by the i-CVD layers.

4. Conclusions and outlook

In this work, the impact of the infiltration of the i-CVD monomer in the residual nano-porosity of SiO_2 barrier layers was investigated with

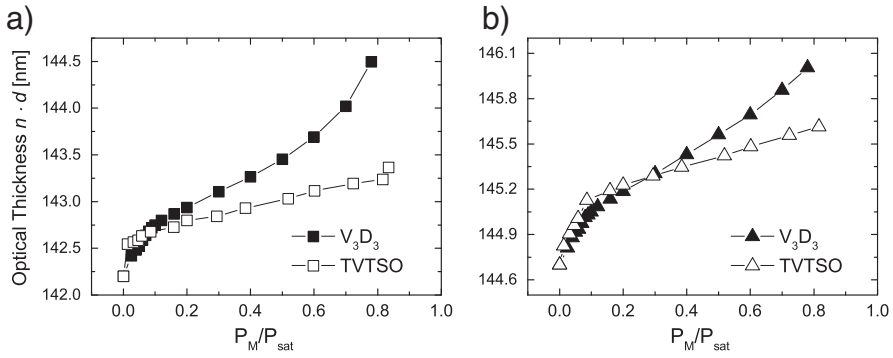

Fig. 4. V_3D_3 and TVTSO adsorption isotherms performed on a) porous ($n_{in\ situ} = 1.422$) and b) dense ($n_{in\ situ} = 1.447$) SiO_2 layers, reported as optical thickness *vs.* P_M/P_{sat}.

respect to the decoupling effect of the defects/pinholes present at the SiO_2 surface. Ca test measurements were able to discern between the water permeation through the defects/pinholes and the permeation through the inorganic layer matrix. The impact of the infiltration of V_3D_3 into the nano-pores was found to be effective only for barriers characterized by an *intrinsic* WVTR value > 10^{-3} g m^{-2} day^{-1}, while, using a smaller molecule, TVTSO, this limit was shifted to WVTR values down to 10^{-5} g m^{-2} day^{-1}. For both organosilicon monomers the BIF was limited to a factor of 4. When the effect of the filling of the nano-pores is compared with the impact of the poly(V_3D_3) in terms of control on the macro-defect density, it is concluded that the main contribution of the i-CVD layer is the decoupling of the defects/pinholes. Considering the limited BIF values here reported, it can be argued that an infiltration into smaller size pores (*i.e.*, <0.85 nm) can provide better moisture permeation barrier levels, as these pores are still accessible to water vapor permeation. Furthermore, a valid approach towards higher *intrinsic* BIF values can consist in selecting monomers showing a hydrophobic character, which would eventually affect the organic interlayer in terms of water solubility and diffusivity, as suggested in the study of Graff [28].

Acknowledgments

The authors would like to thank J. J. A. Zeebregts, M. J. F. van de Sande, J. J. L. M. Meulendijks, H. M. M. de Jong, and W. Keuning for their skillful technical assistance. T. van Mol, J. J. Michels, S. Unnikrishnan, F. J. H. van Assche (Holst Centre, High Tech Campus, Eindhoven, The Netherlands), and P. Klaassen (Philips Research, High Tech Campus, Eindhoven) are kindly acknowledged for the WVTR measurements and the data discussion. The work of A. P. forms part of the research program of the Dutch Polymer Institute (DPI) project #752 and the work of G. A. forms part of the project #663 of the Large Area Thin Film Electronics (LATFE) program. M. C. acknowledges the Aspasia NWO program.

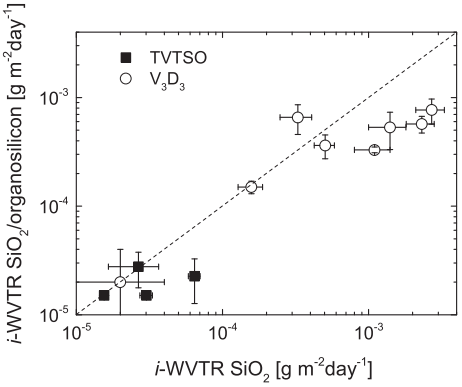

Fig. 5. *Intrinsic* WVTR values of the organosilicon polymer/SiO_2 layer as function of the *intrinsic* WVTR of the SiO_2-*like* layer. Points lying on the dashed line indicate no barrier improvement upon the deposition of the i-CVD layer (BIF = 1). The determination of the *intrinsic* barrier properties for the layer exhibiting a WVTR as low as $3 \cdot 10^{-5}$ g m^{-2} day^{-1} comes with a large error bar because the measurement was limited by the fact that the white spots grew until covering the Ca area used to determine the *intrinsic* barrier properties. However, in both cases the minimum oxidation of 1 nm of Ca to CaO was not reached. Therefore, only upper limit values of WVTR are reported in the graph.

References

[1] U. Soo Lee, J. Sik Choi, B. Seob Yang, S. Oh, Y. Jang Kim, M. Sook Oh, J. Heo, H. Joon Kim, Formation of a bilayer of ALD-SiO_2 and sputtered Al_2O_3/ZrO_2 films on polyethylene terephthalate substrates as a moisture barrier, ECS Solid State Lett. 2 (2013) R13.
[2] P.E. Burrows, G.L. Graff, M.E. Gross, P.M. Martin, M.K. Shi, M. Hall, E. Mast, C. Bonham, W. Bennett, M.B. Sullivan, Ultra barrier flexible substrates for flat panel displays, Displays 22 (2001) 65.
[3] G. Nisato, M. Kuilder, P. Bouten, L. Moro, O. Philips, N. Rutherford, P-88: thin film encapsulation for OLEDs: evaluation of multi-layer barriers using the Ca test, SID Symp. Dig. Tech. Pap., 34 2003, p. 550.
[4] D.A. Spee, J.K. Rath, R.E.I. Schropp, Using hot wire and initiated chemical vapor deposition for gas barrier thin film encapsulation, Thin Solid Films 575 (2014) 67.
[5] C. Tanase, P. van de Weijer, H. Lifka, G. Rietjens, Thin film encapsulated transparent organic light emitting diodes, MRS Proc. 1091 (2008) (1091–AA13–08).
[6] S.P. Subbarao, M.E. Bahlke, I. Kymissis, Laboratory thin-film encapsulation of air-sensitive organic semiconductor devices, IEEE Trans. Electron Devices 57 (2010) 153.
[7] P. van de Weijer, T. van Mol, White paper on the characterisation of thin-film barrier layers for protection of organic light-emitting diodes, ICT-216641 Fast2Light2009. 1.
[8] W. Keuning, P. van de Weijer, H. Lifka, W.M.M. Kessels, M. Creatore, Cathode encapsulation of organic light emitting diodes by atomic layer deposited Al_2O_3 films and Al_2O_3/a-SiNx:H stacks, J. Vac. Sci. Technol., A 30 (2012) 01A131.
[9] K. Vasko, K. Noller, M. Mikula, S. Amberg-Schwab, U. Weber, Multilayer coatings for flexible high-barrier materials, Cent. Eur. J. Phys. 7 (2009) 371.
[10] Y.C. Lee, Atomic layer deposition/molecular layer deposition for packaging and interconnect of N/MEMS, in: S. Garcia-Blanco, R. Ramesham (Eds.), SPIE MOEMS-MEMS, International Society for Optics and Photonics, 2011 (792802–792802–9).
[11] A.A. Dameron, D. Seghete, B.B. Burton, S.D. Davidson, A.S. Cavanagh, J.A. Bertrand, S.M. George, Molecular layer deposition of alucone polymer films using trimethylaluminum and ethylene glycol, Chem. Mater. 20 (2008) 3315.
[12] S.M. George, B. Yoon, A.A. Dameron, Surface chemistry for molecular layer deposition of organic and hybrid organic–inorganic polymers, Acc. Chem. Res. 42 (2009) 498.
[13] M. Park, S. Oh, H. Kim, D. Jung, D. Choi, J.-S. Park, Gas diffusion barrier characteristics of Al_2O_3/alucone films formed using trimethylaluminum, water and ethylene glycol for organic light emitting diode encapsulation, Thin Solid Films 546 (2013) 153.
[14] W. Xiao, D. Yu, S.F. Bo, Y.Y. Qiang, Y. Dan, C. Ping, D.Y. Hui, Z. Yi, The improvement of thin film barrier performances of organic–inorganic hybrid nanolaminates employing a low-temperature MLD/ALD method, RSC Adv. 4 (2014) 43850.
[15] T.W. Kim, M. Yan, A.G. Erlat, P.A. McConnelee, M. Pellow, J. Deluca, T.P. Feist, A.R. Duggal, M. Schaepkens, Transparent hybrid inorganic/organic barrier coatings for plastic organic light-emitting diode substrates, J. Vac. Sci. Technol., A. 23 (2005) 971.
[16] A. Francescangeli, F. Palumbo, R. d'Agostino, Deposition of barrier coatings from vinyltrimethylsilane-fed glow discharges, Plasma Process. Polym. 5 (2008) 708.
[17] G. Dennler, C. Lungenschmied, H. Neugebauer, N.S. Sariciftci, M. Latrèche, G. Czeremuszkin, M.R. Wertheimer, A new encapsulation solution for flexible organic solar cells, Thin Solid Films 511–512 (2006) 349.
[18] J. Fahlteich, M. Fahland, W. Schönberger, N. Schiller, Permeation barrier properties of thin oxide films on flexible polymer substrates, Thin Solid Films 517 (2009) 3075.
[19] A.M. Coclite, G. Ozaydin-Ince, F. Palumbo, A. Milella, K.K. Gleason, Single-chamber deposition of multilayer barriers by plasma enhanced and initiated chemical vapor deposition of organosilicones, Plasma Process. Polym. 7 (2010) 561.
[20] M.E. Alf, A. Asatekin, M.C. Barr, S.H. Baxamusa, H. Chelawat, G. Ozaydin-Ince, C.D. Petruczok, R. Sreenivasan, W.E. Tenhaeff, N.J. Trujillo, S. Vaddiraju, J. Xu, K.K.

Gleason, Chemical vapor deposition of conformal, functional, and responsive polymer films, Adv. Mater. 22 (2010) 1993.
[21] A. Asatekin, M.C. Barr, S.H. Baxamusa, K.K.S. Lau, W. Tenhaeff, J. Xu, K.K. Gleason, Designing polymer surfaces via vapor deposition, Mater. Today 13 (2010) 26.
[22] G. Ozaydin-Ince, A.M. Coclite, K.K. Gleason, CVD of polymeric thin films: applications in sensors, biotechnology, microelectronics/organic electronics, microfluidics, MEMS, composites and membranes, Rep. Prog. Phys. 75 (2012) 016501.
[23] K.K.S. Lau, K.K. Gleason, Initiated chemical vapor deposition (iCVD) of poly(alkyl acrylates): a kinetic model, Macromolecules 39 (2006) 3695.
[24] K.K.S. Lau, K.K. Gleason, Initiated chemical vapor deposition (iCVD) of poly(alkyl acrylates): an experimental study, Macromolecules 39 (2006) 3688.
[25] A.S. da Silva Sobrinho, Transparent barrier coatings on polyethylene terephthalate by single- and dual-frequency plasma-enhanced chemical vapor deposition, J. Vac. Sci. Technol., A 16 (1998) 3190.
[26] J. Affinito, D. Hilliard, A New Class of Ultra-Barrier Materials, Soc. Vac. Coaters 47th Annu. Tech. Conf. Proc 2004, p. 563.
[27] M. Schaepkens, T.W. Kim, A.G. Erlat, M. Yan, K.W. Flanagan, C.M. Heller, P.A. McConnelee, Ultrahigh barrier coating deposition on polycarbonate substrates, J. Vac. Sci. Technol., A 22 (2004) (1716–1722).
[28] G.L. Graff, R.E. Williford, P.E. Burrows, Mechanisms of vapor permeation through multilayer barrier films: lag time versus equilibrium permeation, J. Appl. Phys. 96 (2004) 1840.
[29] Y.G. Tropsha, N.G. Harvey, Activated rate theory treatment of oxygen and water transport through silicon oxide/poly(ethylene terephthalate) composite barrier structures, J. Phys. Chem. B 101 (1997) 2259.
[30] A.G. Erlat, B.-C. Wang, R.J. Spontak, Y. Tropsha, K.D. Mar, D.B. Montgomery, E.A. Vogler, Morphology and gas barrier properties of thin SiOx coatings on polycarbonate: correlations with plasma-enhanced chemical vapor deposition conditions, J. Mater. Res. 15 (2000) 704.
[31] G. Aresta, J. Palmans, M.C.M. van de Sanden, M. Creatore, Evidence of the filling of nano-porosity in SiO_2-like layers by an initiated-CVD monomer, Microporous Mesoporous Mater. 151 (2012) 434.
[32] G. Nisato, P.C.P. Bouten, P.J. Slikkerveer, W.D. Bennett, G.L. Graff, N. Rutherford, L. Wiese, Evaluating high performance diffusion barriers: the Ca test, 21st Annu. Asia Display, 8th Int. Disp. Work 2001, p. 1435.
[33] S. Eslava, F. Iacopi, M.R. Baklanov, C.E.A. Kirschhock, K. Maex, J.A. Martens, Ultraviolet-assisted curing of polycrystalline pure-silica zeolites: hydrophobization, functionalization, and cross-linking of grains, J. Am. Chem. Soc. 129 (2007) 9288.
[34] C. Licitra, R. Bouyssou, T. Chevolleau, F. Bertin, Multi-solvent ellipsometric porosimetry analysis of plasma-treated porous SiOCH films, Thin Solid Films 518 (2010) 5140.
[35] K.S.W. Sing, D.H. Everett, R.A.W. Haul, L. Moscou, R.A. Pierotti, J. Rouquerol, T. Siemieniewska, Reporting physisorption data for gas/solid systems with special reference to the determination of surface area and porosity (Recommendations 1984), Pure Appl. Chem. 57 (1985) 603.
[36] K.S.W. Sing, Characterization of porous materials: past, present and future, Colloids Surf. A Physicochem. Eng. Asp. 241 (2004) 3.
[37] A. Perrotta, E.R.J. van Beekum, G. Aresta, A. Jagia, W. Keuning, M.C.M. van de Sanden, W.M.M. Kessels, M. Creatore, On the role of nanoporosity in controlling the performance of moisture permeation barrier layers, Microporous Mesoporous Mater. 188 (2014) 163.
[38] S.J. Gregg, K.S.W. Sing, Adsorption, Surface Area, and Porosity, Academic Press Inc. Ltd., London, England, 1991.
[39] J. Rouquerol, F. Rouquerol, P. Llewellyn, G. Maurin, K.S.W. Sing, Adsorption by Powders and Porous Solids: Principles, Methodology and Applications, Academic Press, 2013.
[40] G. Aresta, J. Palmans, M.C.M. van de Sanden, M. Creatore, Initiated-chemical vapor deposition of organosilicon layers: monomer adsorption, bulk growth, and process window definition, J. Vac. Sci. Technol., A 30 (2012) 041503.
[41] W.S. O'Shaughnessy, M. Gao, K.K. Gleason, Initiated chemical vapor deposition of trivinyltrimethylcyclotrisiloxane for biomaterial coatings, Langmuir 22 (2006) 7021.
[42] C. Rau, W. Kulisch, Mechanisms of plasma polymerization of various silico-organic monomers, Thin Solid Films 249 (1994) 28.
[43] A.M. Coclite, K.K. Gleason, Initiated PECVD of organosilicon coatings: a new strategy to enhance monomer structure retention, Plasma Process. Polym. 9 (2012) 425.
[44] A.K.H. Achyuta, A.J. White, H.G. Pryce Lewis, S.K. Murthy, Incorporation of linear spacer molecules in vapor deposited silicone polymer thin films, Macromolecules 42 (2009) 1970.
[45] W.S. O'Shaughnessy, S.K. Murthy, D.J. Edell, K.K. Gleason, Stable biopassive insulation synthesized by initiated chemical vapor deposition of poly(1,3,5-trivinyltrimethylcyclotrisiloxane), Biomacromolecules 8 (2007) 2564.
[46] A. Grill, D.A. Neumayer, Structure of low dielectric constant to extreme low dielectric constant SiCOH films: Fourier transform infrared spectroscopy characterization, J. Appl. Phys. 94 (2003) 6697.
[47] T.B. Casserly, K.K. Gleason, Enthalpies of formation and reaction for primary reactions of methyl- and methylmethoxysilanes from density functional theory, Plasma Process. Polym. 2 (2005) 669.
[48] D.D. Burkey, K.K. Gleason, Structure and mechanical properties of thin films deposited from 1,3,5-trimethyl-1,3,5-trivinylcyclotrisiloxane and water, J. Appl. Phys. 93 (2003) 5143.
[49] D.D. Burkey, K.K. Gleason, Temperature-resolved Fourier transform infrared study of condensation reactions and porogen decomposition in hybrid organosilicon-porogen films, J. Vac. Sci. Technol., A 22 (2004) 61.
[50] A. Francescangeli, F. Palumbo, R. d'Agostino, C. Defranoux, Pulsed plasma deposition from vinyltrimethylsilane/oxygen mixtures, Plasma Process. Polym. 6 (2009) 132.
[51] S.H. Baxamusa, K.K. Gleason, Thin polymer films with high step coverage in microtrenches by initiated CVD, Chem. Vap. Depos. 14 (2008) 313.
[52] M. Gupta, V. Kapur, N.M. Pinkerton, K.K. Gleason, Initiated chemical vapor deposition (iCVD) of conformal polymeric nanocoatings for the surface modification of high-aspect-ratio pores, Chem. Mater. 20 (2008) 1646.
[53] C. Bourreau, Y. Catherine, P. Garcia, Growth kinetics and step coverage in plasma deposition of silicon dioxide from organosilicon compounds, Mater. Sci. Eng. A 139 (1991) 376.
[54] M.J. Cooke, Monte Carlo simulation of thin-film deposition in a rectangular groove, J. Vac. Sci. Technol., A 7 (1989) 3217.
[55] L.H. Kim, K. Kim, S. Park, Y.J. Jeong, H. Kim, D.S. Chung, S.H. Kim, C.E. Park, Al_2O_3/TiO_2 nanolaminate thin film encapsulation for organic thin film transistors via plasma-enhanced atomic layer deposition, ACS Appl. Mater. Interfaces 6 (2014) 6731.